Flexural behaviour of the north Algerian margin and tectonic implications

Lamine Hamai, Carole Petit, Abdeslem Abtout, Abdelkarim Yelles-Chaouche, Jacques Déverchère

Geophysical Journal International

Geophys. J. Int. (2015) **201,** 1426–1436 doi: 10.1093/gji/ggv098
GJI Geodynamics and tectonics

Flexural behaviour of the north Algerian margin and tectonic implications

Lamine Hamai,[1,2] Carole Petit,[1] Abdeslem Abtout,[2] Abdelkarim Yelles-Chaouche[2] and Jacques Déverchère[3]

[1] *Geoazur, CNRS-UNS-IRD,* 250 *rue Albert Einstein, F-*06560 *Valbonne-Sophia Antipolis, France. E-mail: lamine.hamai@yahoo.fr*
[2] *Centre de Recherches en Astronomie Astrophysique et Géophysique, Route de l'Observatoire, BP* 63, *Algiers, Algeria*
[3] *Domaines Oceaniques, Institut Européen de la Mer, CNRS-UBO, Technopôle Brest-Iroise, Place Nicolas Copernic, F-*29280 *Plouzané, France*

Accepted 2015 February 24. Received 2015 February 23; in original form 2014 October 15

SUMMARY

The Algerian margin formed through back-arc opening of the Algerian basin (Mediterranean Sea) resulting from the roll-back of the Tethyan slab. Recent geophysical data acquired along the Algerian margin showed evidence of active or recent compressive deformation in the basin due to the ongoing Africa–Eurasia convergence. Published data from four wide-angle seismic profiles have allowed imaging the deep structure of the Algerian margin and its adjacent basins. In this study, we converted these velocity models into density models, then into isostatic anomalies. This allowed us to image an isostatic disequilibrium (relative to a local isostasy model) reaching a maximum amplitude at the margin toe. Converting isostatic anomalies into Moho depth variations shows that the Moho extracted from wide-angle seismic data is deeper than the one predicted by a local isostasy model in the oceanic domain, and shallower than it in the continental domain. These anomalies can be interpreted by opposite flexures of two plates separated by a plate boundary located close to the margin toe. We use a finite element model to simulate the lithospheric flexure. The amplitude of the equivalent vertical Moho deflection is larger in the central part of the study area (6–7 km) than on the easternmost and westernmost profiles (3 km). The effective elastic thickness used to best match the computed deflection is always extremely low (always less than 10 km) and probably reflects the relatively low strength of the lithosphere close to the plate boundary. Comparison with other wide-angle seismic profiles across an active and a passive margin show that the North Algerian margin displays isostatic anomalies close to that of an active margin. Finally, plate flexure is highest at the southern tip of the ocean-continent transition, possibly indicating that a former passive margin detachment is reactivated as a crustal scale reverse fault pre-dating a future subduction.

Key words: Gravity anomalies and Earth structure; Continental margins: convergent; Dynamics of lithosphere and mantle; Lithospheric flexure; Crustal structure.

1 INTRODUCTION

Whereas oceanic subduction is one of the most important processes of plate tectonics, understanding how and where it begins is still a matter of debate, mostly because examples of incipient oceanic subduction worldwide are scarce (e.g. Gerya 2011, and references therein). The transition from passive to active margin can result from various phenomena, including buoyancy contrasts, thermal instability of the oceanic lithosphere, differential surface loading due to erosion and deposition, body forces or other parameters (e.g. Gurnis 1992; Faccenna *et al.* 1999; Regenauer-Lieb *et al.* 2001; Niu *et al.* 2003; Zhu *et al.* 2009). Commonly, subduction initiation mechanisms are assumed to fall into two categories (Stern 2004, and references therein): induced or spontaneous, depending on whether they are driven by the far-field tectonic plate motions or by local gravitational instabilities. In all cases, most numerical models of subduction initiation require a pre-existing weakness zone in which deformation is located (Gerya 2011, and references therein). However, the actual structures of this weak zone, its origin, and its relationship with the early stages of compressional deformation are still unclear. Deciphering the structure of a recently inverted passive or transform margin can thus help understanding how induced subduction initiates and localizes.

The Algerian basin is a young oceanic basin (∼20 Ma or less, Schettino & Turco 2006, 2011; van Hinsbergen *et al.* 2014) undergoing compressive boundary conditions due to Africa–Eurasia

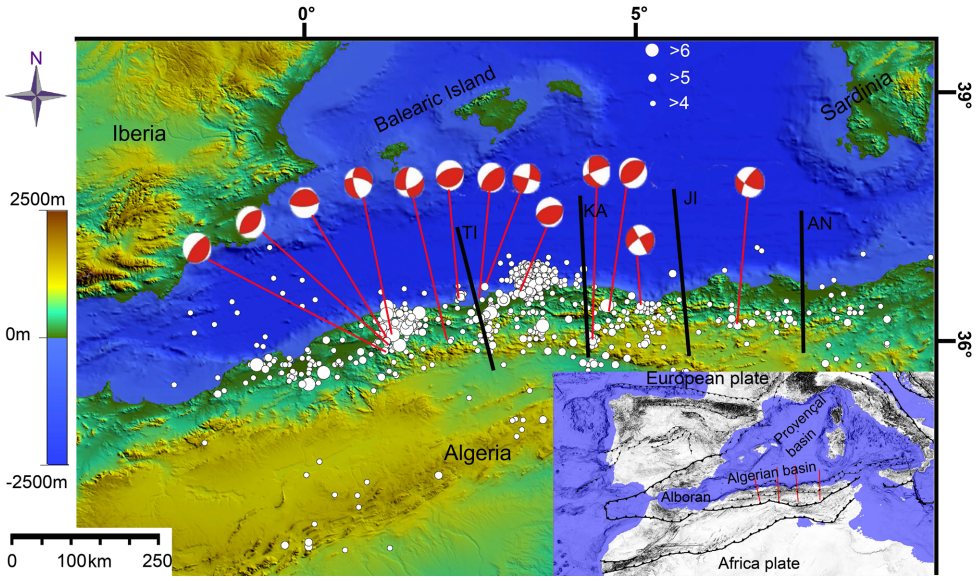

Figure 1. Topography, bathymetry by ETOPO1 1-min global relief (www.ngdc.noaa.gov) and seismicity of the Algerian margin (epicentres and focal mechanisms). Solid lines indicate the location of the SPIRAL wide-angle profiles. Inset shows a more regional tectonic sketch of the Mediterranean Region (modified after Barrier *et al.* 2004).

convergence at a rate of less than ~1 cm yr^{-1} (Dewey *et al.* 1989; Serpelloni *et al.* 2007; Carminati *et al.* 2012). These kinematic boundary conditions favor subduction inception along the North African margin (Cloetingh *et al.* 1982, 1989). Northern Algeria, located at the Africa–Eurasia Plate boundary south of the Algerian basin, currently undergoes a slow compressional deformation on its continental margin (Auzende *et al.* 1972; Frizon de Lamotte *et al.* 2011), as evidenced by active seismicity recorded both on land and at sea (Domzig *et al.* 2006; Yelles-Chaouche *et al.* 2006; Kherroubi *et al.* 2009; Kherroubi 2011). This recent compression (of which the onset is dated between 10 and 2 Ma) between Eurasia and Africa has been proposed earlier (e.g. Le Pichon 1968; Talwani *et al.* 1969; Caputo *et al.* 1970; McKenzie *et al.* 1970), however from Gibraltar to Sicily, the precise geometry of the plate boundary is still poorly defined, because the deformation is still diffuse and not yet localized on a well-defined plate interface. The North African margin in Algeria may therefore represent a transitional stage between active and passive margin settings (Lonergan & White 1997; Gueguen *et al.* 1998; Rosenbaum *et al.* 2002a; Faccenna *et al.* 2004; Mauffret *et al.* 2004; Jolivet *et al.* 2006, 2009; Yelles *et al.* 2009; Carminati *et al.* 2012). If this was the case, then the lithosphere should display an isostatic signal close to that of mature subduction zones, that is, a progressive downward bending of the oceanic plate towards the continental margin that is not due to a 'normal' plate deflection under its own load.

In this study, we use recently published 2-D velocity models computed from wide-angle seismic data of the SPIRAL 2009 survey on the North Algerian margin (Aidi *et al.* 2013; Leprêtre *et al.* 2013; Mihoubi *et al.* 2014; Bouyahiaoui *et al.* 2015). The velocity structure is converted into a density structure and an isostatic analysis is performed by comparing measured (from merged data sets) and computed gravity anomalies. Isostatic anomalies are modelled using a broken elastic plate model. From these results, we aim (1) to test whether a flexural effect is indeed detectable along the Algerian margin, (2) if so, to evidence the along-strike changes of flexure and of mechanical properties of the oceanic lithosphere and (3) to discuss their origin by comparison with other types of margins worldwide.

2 SUMMARY OF GEODYNAMICAL HISTORY

The Western Mediterranean Sea belongs to the Alpine orogenic system and is located near the boundary of Africa and Eurasia plates. The western Mediterranean basin depicts a unique, complex structure, with its steep mountain ranges and large continental island blocks which separate several sub-basins (Fig. 1).

During the Liassic, the opening of the central Atlantic caused a sinistral strike-slip motion between Africa and Iberia, creating a transform zone passing through the Gibraltar strait (Roca *et al.* 2004). Approximately at the same time, the dislocation of Pangea led to the opening of the Alpine Tethys (Irving 1977, 2004; Muttoni *et al.* 1996; Frizon de Lamotte *et al.* 1991, 2011). The northern Tethyan passive margin is born at the southern edge of the AlKaPeCa (Alboran Kabylia Peloritan and Calabria, Bouillin 1986) continental block system, itself attached to the Sardinia and Balearic proto-islands. In the Late Cretaceous (84 Ma, e.g. Gelabert *et al.* 2002), the motion of the African plate changed due to the opening of the South Atlantic, causing the onset of convergence between Europe and Africa (Olivet *et al.* 1982; Dewey *et al.* 1989; Ricou 1996; Rosenbaum *et al.* 2002a; Cavazza *et al.* 2004; Schettino & Turco 2011). This new stress regime initiated the closure of the Tethys Ocean, which was accommodated in the Maghreb by northward subduction and opening of the Algerian backarc basin between stable Eurasia and AlKaPeCa microcontinents. This stage ended with the collision between the continental AlKaPeCa blocks and Africa (Lonergan & White 1997; Gueguen *et al.* 1998; Roca *et al.* 1999; Verges & Sabat 1999; Frizon de Lamotte *et al.* 2000; Faccenna *et al.* 2001; Roca 2001; Rosenbaum *et al.* 2002a; Mauffret *et al.* 2004). These continental blocks, initially belonging to the European margin (Bouillin 1986), broke up into several sub-blocks that migrated southward and formed the internal zones of the Alpine south-Mediterranean belt after their collision with North Africa. A two-stage kinematic model of opening of the Algerian basin has been proposed, with a first N–S opening due to the southward migration of the AlKaPeCa blocks at 35 Myr, followed by an EW opening with the formation of oceanic crust along NS trending accretionary

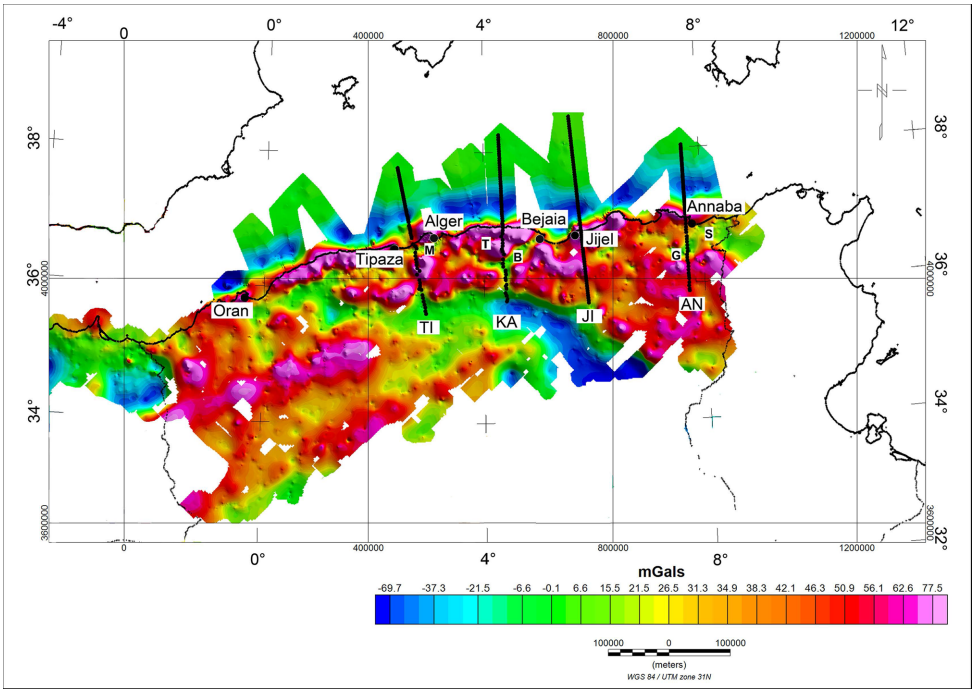

Figure 2. Free air anomaly map of northern Algeria. Solid lines mark the SPIRAL wide-angle seismic profiles (TI = Tipaza, KA = Greater Kabylia, JI = Jijel, AN = Annaba).

centres between 16 and 8 Myr (Mauffret *et al.* 2004; Mauffret 2007; van Hinsbergen *et al.* 2014). According to this hypothesis, the late stage of opening of the basin is associated with the westward migration of the Gibraltar Arc and eastward migration of the Calabrian arc, and occurred after the collision of the Kabylian massifs with North Africa. Magmatism attributed to slab detachment occurred first in the Langhien (∼15 Ma) at the central Algerian coast and then spread to the west and east, supporting the hypothesis of opposite migration of the Calabrian and Gibraltar slab tears (Carminati *et al.* 1998; Maury *et al.* 2000; Savelli 2002; Spakman & Wortel 2004). Nowadays, the still ongoing Africa–Europe convergence is recorded in Algeria, both in the coastal basins on land (e.g. the Chelif and Mitidja basins) and in the offshore, with characteristic fold-thrust structures (Boudiaf 1996; Déverchère *et al.* 2005; Domzig *et al.* 2006; Yelles-Chaouche *et al.* 2006; Kherroubi *et al.* 2009; Yelles *et al.* 2009).

3 AVAILABLE DATA SETS

In order to quantitatively assess the mechanical properties at the plate boundary, several terrestrial and marine gravity data sets from the 'Bureau Gravimétrique International (BGI, International Gravimetric Bureau 2012), http://bgi.obs-mip.fr' database were used. This database consists of irregularly spaced points issue from some of survey, attached to different gravity bases (Bouyahiaoui *et al.* 2011). Its accuracy is estimated at 1 mGal and the measurements are attached to the 1930 Potsdam network (Idres & Aifa 1995).

In order to use the BGI data, it was essential to bring all data survey to the same level of reference (for the data to be homogeneous). For this purpose, we used the new gravity measurements acquired in the framework of missions CRAAG at places where BGI data existed (Abtout *et al.* 2014). Comparison of old data to new measurements allowed us to compute a systematic offset due to different attachments. This difference was added to the old values to bring them to the same reference ellipsoid as the absolute measurements.

In a second step, outliers were eliminated by a systematic search of peaks outside the mean distribution, centred on a square of 100 km × 100 km. These treatments provided a self-consistent free-air anomaly map attached to the absolute gravity reference bases.

The resulting free air anomaly map shows several positive anomalies on the northern of continental margin, and negative anomalies representing the sedimentary basins (Fig. 2). The latter are namely, the backarc Mitidja basins near Algiers, the Tizi Ouzou basin and the small basins of Guelma and Seybouse in the East near Annaba. Positive anomalies on the continental domain are limited to the north by negative anomalies representing the limit of the margin. Some positive anomalies however extend offshore, in the Kheir Eddine bank in Algiers, and the Edough massif near Annaba.

Free air anomaly profiles were then drawn along four wide-angle seismic profiles of the SPIRAL survey (Tipaza, Greater Kabylia, Jijel and Annaba profiles from west to east, Fig. 2), in order to provide a first-order check on the velocity model determined by forward inversion of wide-angle data (Aidi *et al.* 2013; Leprêtre *et al.* 2013; Mihoubi *et al.* 2014; Bouyahiaoui *et al.* 2015).

4 METHODS

For each of the four profiles, the final velocity model computed from wide-angle seismic forward modelling was converted into a regular 5 km × 1 km velocity V grid using a linear interpolation method. We convert it into a density ρ profile using two different velocity–density conversion rules in order to test the sensitivity of our models to the velocity–density conversion factor.

We first use three different velocity–density conversions for the sediments, upper crust and deep crust and mantle, using Hamilton

(1978), Carlson & Herrick (1990) and Birch (1961) laws, such as, respectively:

$$\rho = 1 + 1.18(V - 1.5)^{0.22}$$

$$\rho = 3.61 - \frac{6.0}{V}$$

$$B = \frac{\mathrm{d}V}{\mathrm{d}\rho}. \quad (1)$$

For the Birch law, we choose a B factor of 2.8 and an integration constant of –1.45 in order to retrieve commonly accepted density values of 1030 and 3300 kg m^{-3} for the water and uppermost mantle, respectively. The second conversion model uses the Birch law for all crust and mantle rocks. The velocity–density conversion is different for the salt layer, for which the density is of 2200 kg m^{-3} for seismic velocities ranging between 3.9 and 4.1 km s^{-1}. The density models are then used to calculate a theoretical gravimetric anomaly that can be compared to the measured one.

We then test if the profiles are in local isostatic equilibrium in an Airy sense. If this was the case, then the weight of each vertical column should be the same all along the profile. For each longitudinal profile node, the weight $P(x)$ of the column of crust and mantle are computed such as:

$$P(x) = \sum_{z=0}^{Z} g\rho(x, z)h, \quad (2)$$

Where h is the height of the grid element (constant), g the gravitational acceleration and Z is the compensation depth (taken as the deepest point of the profile). Relative weight anomalies $\Delta P(x)$ are computed along the profile by subtracting an average to the computed column weights. These anomalies can be interpreted as deviations from the local isostatic equilibrium in the Airy sense. Positive deflection means that the lithosphere is heavier than predicted by an Airy-type model, which can be interpreted for instance as an upward flexure resulting in a Moho uplift and mantle emplacement at crustal levels.

We convert these 'weight anomalies' in an equivalent deflection of the Moho Δh_{moho} with:

$$\Delta h_{\mathrm{moho}} = -\Delta P(\rho_{\mathrm{m}} - \rho_{\mathrm{c}}), \quad (3)$$

where ρ_{m} and ρ_{c} are the upper mantle and crust densities, respectively. Δh_{moho} is therefore the amount of deflection that should be substracted from the observed Moho to bring it to an isostatically compensated ('unflexed') position. We then model this calculated deflection using a thin elastic plate model and a trial and error approach. In this model, the plate bends under the effect of vertical loads and/or moments, which cause the observed plate deflection. Here, all vertical loads due to density changes within the crust are already taken into account by the isostatic analysis, and we seek modelling an 'additional' Moho deflection due to external plate bending forces. The flexure w of a thin elastic plate in 1-D under an applied load q depends on its rigidity D such as:

$$D\frac{\mathrm{d}^4 w}{\mathrm{d}x^4} + (\rho_{\mathrm{m}} - \rho_{\mathrm{c}})gw = q(x), \quad (4)$$

where D is the lithosphere rigidity connected to the effective elastic thickness Te:

$$D = \frac{E.Te^3}{12.(1 - \nu^2)} \quad (5)$$

With E and ν the Young's modulus and the Poisson coefficient, respectively. In a mechanically couple lithosphere, Te is simply the sum of the elastic thicknesses of the crust and mantle. If they are mechanically decoupled, Te writes (Burov & Diament 1995):

$$Te = \left(h_{\mathrm{mant}}^3 + h_{\mathrm{crust}}^3\right)^{1/3}, \quad (6)$$

where h_{crust} and h_{mant} are the crust and mantle elastic thicknesses, respectively.

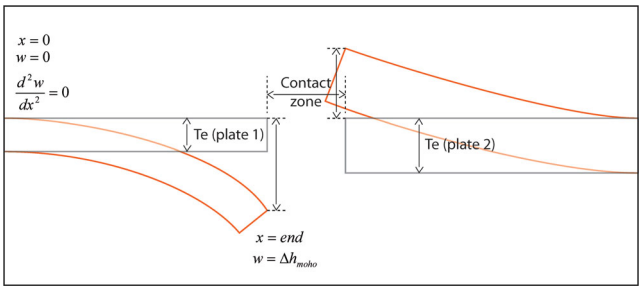

Figure 3. Setup of the flexural models. *Te* is the effective elastic thickness in km. The deflection (w) is set to zero at the extremities of the plates, and imposed at the plate junction.

A finite element formulation is used to model the lithospheric flexure at the plate boundary (Kwon & Bang 2000). The profiles are discretized into two distinct plates for the continental and oceanic parts, which allow us to apply opposite flexures on both domains. The two plates can be separated by a transition zone of variable width where no flexure is computed. This transition zone is a free slip boundary, that is, each plate can move independently from the other one. We have focused our study on the oceanic part because the continental domain is less well constrained due to the lack of seismic shots on land. The deflection and the plate curvature oppositely to their point of junction ($x = 0$) are set to zero, and the amount of deflection computed from the equivalent Moho deflection is applied at both ends of each plate ($x =$ end), such as (Fig. 3):

$$w_{(0)} = 0$$

$$\left.\frac{\mathrm{d}^2 w}{\mathrm{d}x^2}\right|_{(0)} = 0$$

$$w_{(\mathrm{end})} = \Delta h_{\mathrm{moho(end)}}. \quad (7)$$

The misfit (in km) between the computed flexure and the modelled one is calculated given by the rms value:

$$\mathrm{rms} = \sqrt{\frac{1}{N}\sum_{i=0}^{N}(w_i^{\mathrm{obs}} - w_i^{\mathrm{calc}})^2}, \quad (8)$$

where N is the number of points, w^{obs} is the observed flexure and w^{calc} is the flexure calculated using the finite element method. In all our models, the effective elastic thickness is assumed constant. The main reason is that the seismic profiles are short compared to the characteristic wavelength of flexural response. As a consequence, we are able to determine only the effective elastic thickness of the lithosphere close to the plate boundaries, which is probably much lower than the overall plate rigidity (because of local plate weakening due to tectonic deformation and bending stresses). Introducing a plate variable rigidity on such short profiles would rather help us fitting a noise than a true signal in the plate flexure.

5 MODELLING RESULTS

We present in this section the results of gravity, isostasy and flexure modelling of each profile from west to east (Figs 4–7, and

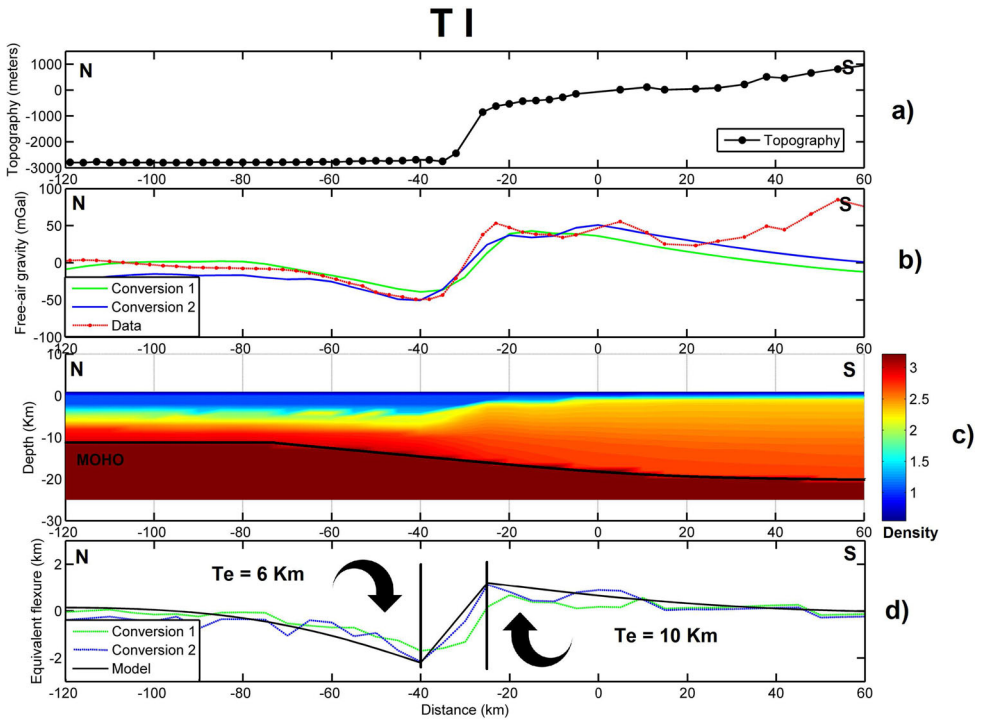

Figure 4. (a) Topography and bathymetry for the Tipaza profile. (b) Free-air anomaly. Dotted red line corresponds to measured gravity. Solid green and blue lines are predicted free-air anomalies using different parameters for the sediments, the upper crust, and the lower crust and mantle (Conversion 1) or using only Birch's law (conversion 2), respectively. (c) Density model calculated by converting the seismic velocities into densities with Birch's law (seismic velocities after Leprêtre *et al.* 2013). (d) 2-D flexural model of the Tipaza profile. Green and blue lines are the computed deflection corresponding to the two different velocity–density conversions, and black line is the modelled deflection. Thick vertical lines delimitate the transition zone between the two flexed plates.

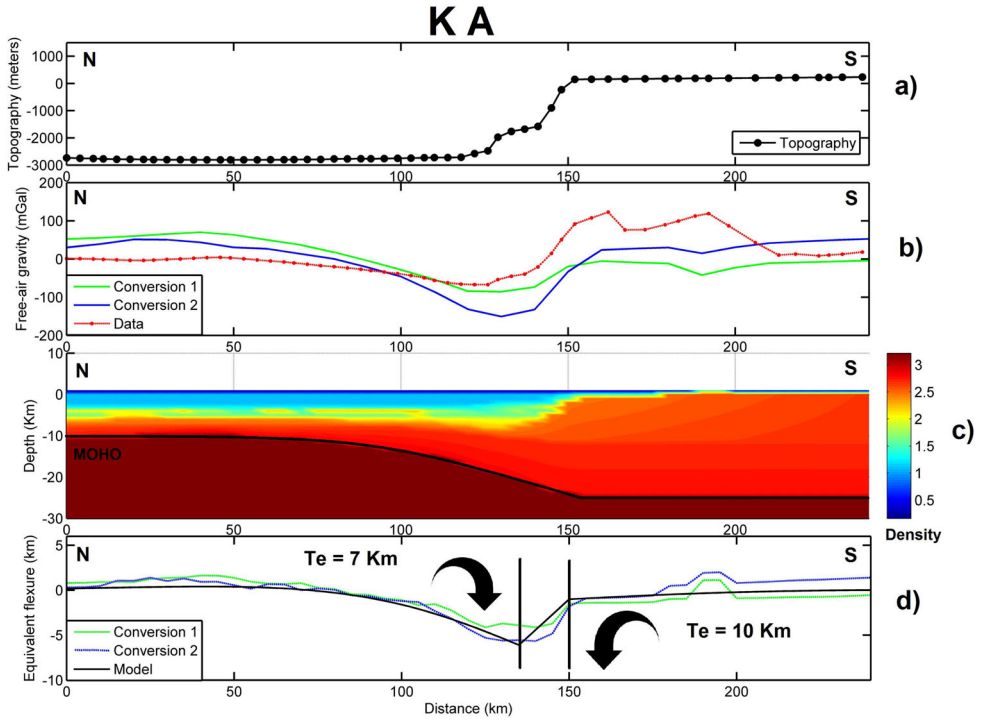

Figure 5. Same legend as Fig. 4 for the Greater Kabylia profile. Seismic velocities after Aidi *et al.* (2013).

Supporting Information 1–4). For each profile, the velocity/density conversion provides slightly different results depending on the conversion method: the first method which uses Hamilton (1978), Carlson & Herrick (1990) and Birch (1961) laws for the sediments, upper crust, and lower crust and mantle, respectively, gives a lower gravity anomaly (by about 10–50 mGal) and a lower amplitude of equivalent deflection (0.5–1 km) than the second method which uses the Birch law only. Despite some discrepancies, the second conversion

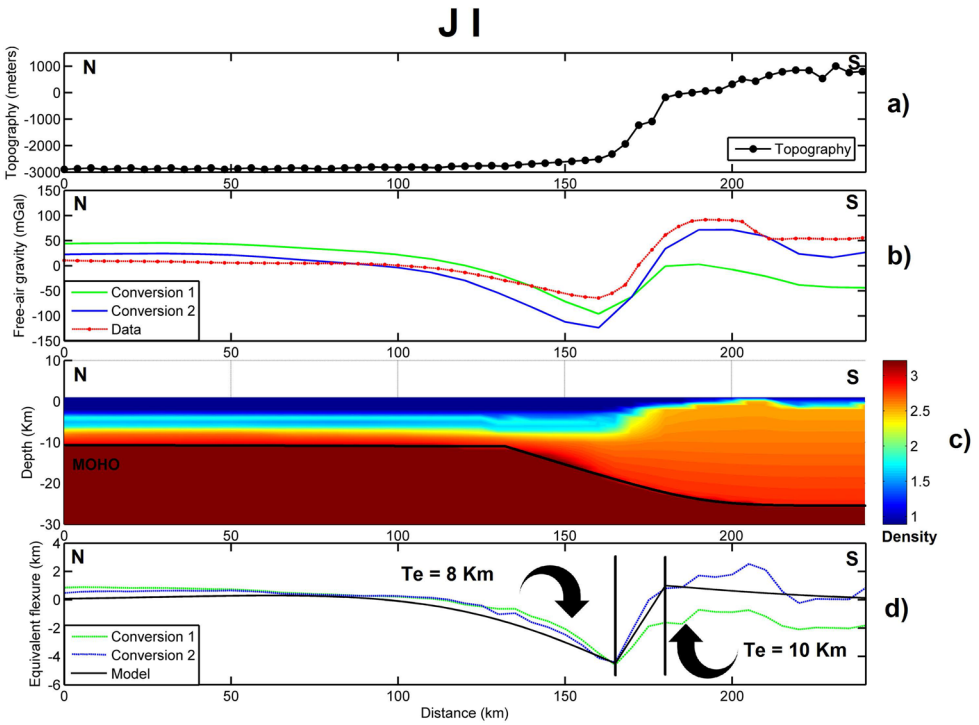

Figure 6. Same legend as Fig. 4 for the Jijel profile. Seismic velocities after Mihoubi *et al.* (2014).

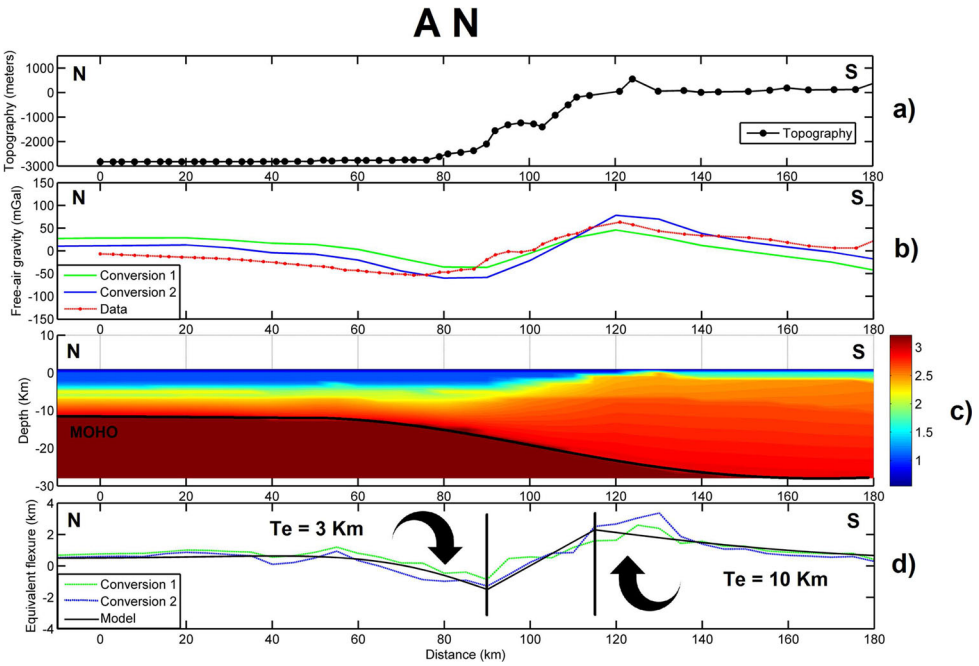

Figure 7. Same legend as Fig. 4 for the Annaba profile. Seismic velocities after Bouyahiaoui *et al.* (2015). Discrepancies between both methods can be used as an estimate of the mean error on the resulting equivalent deflection (i.e. 0.1–1 km). Sensitivity tests allowed us to estimate an uncertainty in the mean effective elastic thickness of about 1 km (Table 1).

method gives generally a best fit to observed gravity data (especially a better fit to the amplitude of the observed gravity anomaly) than the first one, suggesting that the Birch law provides a satisfying velocity–density conversion in our case study (Figs 4b, 5b, 6b and 7b). Whereas the fit to gravity data is satisfying for Tipaza and Annaba profiles, it is not very good for the two central profiles (Greater Kabylia and Jijel). This is probably due to side effects of the Greater Kabylia massif located close to this profile, which affects the gravity signal but not the seismic velocity model on the 2-D profile, or to deeper mantle anomalies sometimes suggested (Cavazza *et al.* 2004; Spakman & Wortel 2004). On both profiles indeed, the observed free-air anomaly signal is tilted counter-clockwise with respect to the modelled ones, suggesting the presence of a long-wavelength 3-D trend in the gravity signal. As a matter of fact, the Birch law predicts a free-air anomaly that is of the same amplitude as the observed one (i.e. about 150 mGal), whereas the free-air

Table 1. Flexural parameters for the 4 modelled profiles, with the amplitude of the imposed deflection at the oceanic plate boundary and the best-fitting effective elastic thickness determined from rms analysis.

Profile	Tipaza	Greater Kabylia	Jijel	Annaba
Amplitude of downward oceanic flexure (km)	2 ± 1	6.1 ± 0.5	4.5 ± 0.5	2 ± 1
Best-fitting *Te* (km)	6 ± 1	7 ± 1	6 ± 1	3 ± 1
Rms conversion 1 (km)	0.33	0.80	0.45	0.72
Rms conversion 2 (km)	0.23	0.48	0.31	0.36

anomaly predicted by the first conversion method is of much lower amplitude (less than 100 mGal). For this reason, we chose to keep the second conversion method (Birch's law only) for all profiles.

5.1 Tipaza profile

The computed deflection shows a clear undercompensation (mass excess) on the continental part and overcompensation (mass deficit) beneath the oceanic domain (Fig. 4c). Moreover, departure from local equilibrium increases exponentially when approaching the ocean–continent transition, both on the continental and oceanic parts. For the flexural model, the parameters of the continental plate are set to an elastic thickness of 10 km, because of the lack of constraints on the crustal structure, and a deflection of –1.2 km is imposed at the plate end. For the oceanic plate, the deflection is set at 2.2 km at the plate end and we calculated the rms for several elastic layers of different thicknesses between 3 and 7 km (Table 1). The elastic thickness which gives the best fit between observed and modelled data is 6 ± 1 km. The width of the transition zone (i.e. between the continental and oceanic plates) in this profile is 20 km (between km-40 and km-20).

5.2 Greater Kabylia profile

Like for the Tipaza profile, the deflection model (Fig. 5c) shows overcompensation on the oceanic crust; however, the isostatic signal is much less clear on the continental part. We set the parameters of the continental plate to an elastic thickness of 10 km and a deflection at 1.2 km is imposed at the point located at 150 km from the beginning of the profile, but this remains unconstrained. For the oceanic plate, we set the deflection at 6 km and we calculated the rms for several elastic layers of different thicknesses between 4 and 10 km (Table 1). The elastic thickness which gives the best fit between observed and modelled data is 7 ± 1 km. The width of the transition zone in this profile is 20 km (between km-130 and km-150).

5.3 Jijel profile

The computed deflection also shows a clear overcompensation (downward flexure) on the oceanic part, increasing towards the foot of the margin, like for the two former profiles (Fig. 6c). The continental part does not display any clear isostatic anomaly but, like for the previous profiles, the velocity model is poorly constrained. We set the parameters of the continental plate to an elastic thickness of 10 km and a deflection of –1 km (km 160), whereas for the oceanic plate, we set the deflection at 4.5 km and tested different *Te* values between 4 and 10 km (Table 1). The elastic thickness which gives the best fit between observed and modelled data is 8 ± 1 km. The width of the transition zone in this profile is 15 km (between 165 and 180 km).

5.4 Annaba profile

The computed deflection along this profile shows a slight overcompensation (downward flexure) on the oceanic part, increasing towards the foot of the margin, and an undercompensation on the continental domain (Fig. 7c). We set the parameters of the continental plate to an elastic thickness of 10 km and a deflection of –2.8 km, whereas for the oceanic plate, we set the deflection at 2 km and tested different *Te* values between 2 and 7 km (Table 1). The elastic thickness which gives the best fit between observed and modelled data is 3 km. The width of the transition zone in this profile is 25 km (between km-90 and km-115).

5.5 Comparison with active and passive margin settings

By comparing Figs 4–7, it appears that the wavelength and amplitude of the downward bending of the oceanic lithosphere in the Algerian basin are larger for the two central profiles (4–6 km) than for the eastern and western ones (1–2 km). In order to assess whether the observed lithosphere deflection is more representative of an active or passive margin setting, we compare our results on the Greater Kabylia profile (considered here as depicting a characteristic flexural profile) to two other wide-angle seismic profile acquired on a typical passive margin, in the Atlantic offshore central Morocco, and across the Sumatra passive margin (Fig. 8, Contrucci *et al.* 2004; Klingelhoefer *et al.* 2009, 2010).

Exactly the same processing as for Algerian profiles was applied in order to obtain 'weight' anomalies which are then converted into an equivalent Moho deflection. The passive margin profile across central Morocco displays an irregular pattern of positive and negative isostatic anomalies, no clear deflection is visible. On the opposite, the plate deflection is well depicted on the Sumatra profile

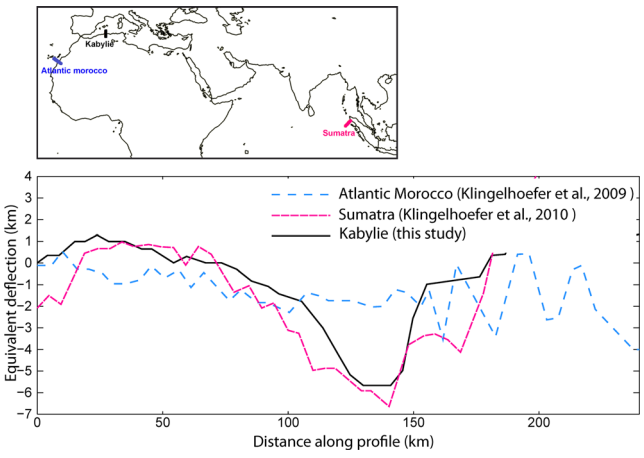

Figure 8. Comparison between the deflection profiles for a typical passive margin offshore central Morocco, an active margin offshore Sumatra, and the Greater Kabylia profiles. Morocco and Sumatra profiles were computed after Klingelhoefer *et al.* (2009, 2010).

where it reaches more than 6 km at the trench. This comparison shows that the Greater Kabylia profile in Algeria, where plate deflection is the largest, has an isostatic signature very similar to that of a typical subduction margin, although no oceanic slab is presently accommodating the Africa–Europe convergence off Algeria.

6 DISCUSSION

By converting isostatic anomalies into Moho depth variations across four segments of the present-day Algerian margin, we show that the Moho extracted from wide-angle seismic data is deeper than the one predicted by a local isostasy model in the oceanic domain, and shallower than it in the continental domain. These anomalies can be interpreted at first order by opposite flexures of two converging plates characterized by effective elastic thicknesses (*Te*) ranging between 3 and 7 km for the oceanic lithosphere. We find no systematic trend in *Te* variations is observed along the margin, although it is worth noting that for the westernmost profile, *Te* is twice lower than for the other ones (3 km instead of 6–7 km). These *Te* values are unexpectedly low for an oceanic lithosphere (Watts & Burov 2003), even only 20 Myr old. However, our profiles are rather short (∼200 km), so we can only reproduce the short wavelength component of the plate flexure, close to the plate boundary. Therefore, these low *Te* values are most likely underestimated. Furthermore, these low values may also reflect a local weakening of the oceanic crust, either by flexural stresses or by tectonic or thermal processes: indeed, the collision of the Inner Zones (AlKaPeCa blocks) with the African margin at *ca*. 19 Ma has been followed by a lateral slab detachment of opposite directions (see Part 1), a process which has induced a migrating volcanic activity near the margin (Maury *et al.* 2000) and has likely weakened the overlying lithosphere.

The amplitude of downward flexure is slightly different from one profile to another, depending on their position along the coast. These changes could be (at least partly) related to the difference in geometry of the margin segments and their regional geodynamic and kinematic evolution that is likely polyphased and strikingly different from east to west (e.g. Medaouri *et al.* 2014; van Hinsbergen *et al.* 2014).

The different models display a transition zone between continental-upward and oceanic-downward flexed plates. This zone is approximately 20 km wide and is shifted to the south (of *ca.* 20 km) with respect to the location of the ocean–continent transition as depicted by velocity models (Fig. 9).

Hence, the plate discontinuity where plate flexure localises at depth (i.e. close to the Moho) locates slightly south of the ocean–

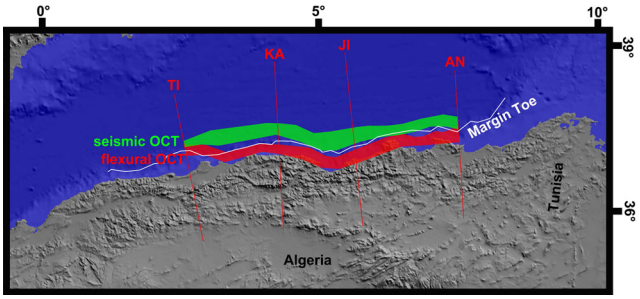

Figure 9. Map location of the transition zone (in red) between the two flexed plates compared with the position of the OCT (ocean-continent transition) (in green) as defined by seismic velocities identified on each profile (thin red lines). The shape of the transition zone is interpolated between the different profiles following the general margin geometry.

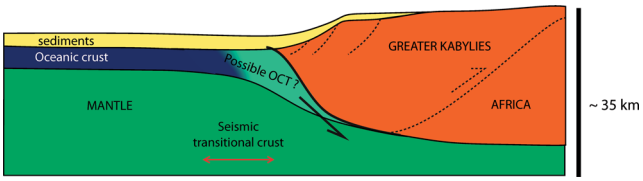

Figure 10. Interpretative cross-section of the present-day deformation on the north Algerian margin, involving a possible detachment reactivation on top of the former OCT, schematically drawn based on structure and seismic interpretation of the Jijel profile (Mihoubi *et al.* 2014).

continent transition (OCT) as identified on the velocity models. If the OCT, like on classical magma-poor passive margins, results from mantle exhumation along a detachment fault (e.g. Brun & Beslier 1996), then this observation suggests that the margin inversion localises on a south-dipping structure that might well be the former detachment along which the mantle was exhumed during the passive margin formation (Fig. 10). Whether this formation was accompanied or not by the development of a margin-parallel STEP fault (Leprêtre *et al.* 2013; Medaouri *et al.* 2014) is difficult to assess from this study, as this kind of fault could also play the role of a major lithospheric weakness during margin inversion. Although in a quite different context, detachment reactivation as a major thrust during rift basin inversion has also been documented in the Pyrenees (Lagabrielle *et al.* 2010; Jammes & Huismans 2012). The north Algerian margin could thus be one of the rare examples of passive margin inversion where extensional detachment is reactivated in compression as a proto-subduction interface, favouring the ongoing underthrusting of the Neogene oceanic domain below the Algerian continental margin (Auzende *et al.* 1975; Déverchère *et al.* 2005).

7 CONCLUSION

Based on accurate velocity models and a new grid of gravity data, the flexure and the mechanical properties of the oceanic lithosphere across the Algerian margin, located at the boundary between Africa and Eurasia plates, were modeleld. Our results show that in the oceanic domain of the Algerian basin, the ‘weight’ of a given column of lithosphere tends systematically to decrease exponentially when approaching the foot of the North African continental margin. Conversely, in the continental area, this ‘weight’ increases when approaching the margin, although this is not strongly constrained. These weight changes show that the profiles (and hence, the foot of the margin) are not in equilibrium in a local sense: if we convert these weight anomalies into variations of Moho depth, then the oceanic Moho becomes increasingly deeper, and the continental Moho increasingly shallower, on either side of a discontinuity located at the margin toe. The isostatic signature of these profiles is thus typical of broken plates with opposite flexures (e.g. Watts 1981, 1992, 2001). The conversion of the‘weight anomaly’ into an equivalent flexure of the Moho shows that the Moho is flexed downward in the oceanic domain for all the four modelled profiles, and probably upward in the continental area at least for two of them. The amplitude of the equivalent deflection is larger in the central part of the study area (4–6 km) than on the easternmost and westernmost profiles (2 km). The effective elastic thickness used to best match the computed deflection is always extremely low (always less than 10 km) and probably reflects the relatively low strength of the lithosphere close to the plate boundary. Finally, plate flexure localises at the southern tip of the OCT, suggesting that the former passive

margin detachment is reactivated as a crustal-scale reverse fault pre-dating a future subduction of the Neogene oceanic lithosphere.

ACKNOWLEDGEMENTS

We thank the teams of the SPIRAL Project, on land and at sea, for their huge work that allowed us to collect the seismic data set used in this study. We benefited from the input by Frauke Klingelhoefer for the use of seismic data and comparison with other margins. Editor Stéphane Labrosse, Laurent Jolivet and an anonymous reviewer are thanked for their constructive and positive reviews.

REFERENCES

Abtout, A., Boukerbout, H., Bouyahiaoui, B. & Gibert, D., 2014. Gravimetric evidences of active faults and underground structure of the Cheliff seismogenic basin (Algeria), *J. Afr. Earth Sci.,* doi:10.1016/j.jafrearsci.2014.02.011.

Aidi, C. *et al.*, 2013. Deep structures of the Algerian continental margin in the Great kabylies- Insights from wide-angle seismic modeling, AGU2013. T21A-2522. Continental Rifts and Rifted Margins, Posters. CONTROL ID: 1794050.

Auzende, J.M., Olivet, J.L. & Bonnin, J., 1972. Une structure compressive au nord de l'Algérie, *Deep Sea Res.,* **19,** 149–155.

Auzende, J.M., Bonnin, J. & Olivet, J.L. 1975. La marge nord-africaine considérée comme marge active, *Bull. Soc. Géol. Fr.,* **17,** 486–495.

Barrier, E., Chamot-Rooke, N. & Giordano, G., 2004. Geodynamic maps of the Mediterranean: tectonics and kinematics (1:3.000.000 scale), Commission for the Geological Map of the World (CGMW).

Birch, F., 1961. The velocity of compressional waves in rocks to 10 kilobars, part 2, *J. geophys. Res.*, **66,** 2199–2224.

Boudiaf, A., 1996. Etude sismotectonique de la région d'Alger et de la Kabylie (Algérie): Utilisation des modèles numériques de terrain (MNT) et de la télédétection pour la reconnaissance des structures tectoniques actives: contribution à l'évaluation de l'aléa sismique, *PhD thesis*, Université Montpellier II, 274 pp.

Bouillin, J.P., 1986. Le bassin Maghrébin : une ancienne limite entre l'Europe et l'Afrique à l'ouest des Alpes, *Bull. Soc. Géol. Fr.,* **8,** 547–558.

Bouyahiaoui, B., Djeddi, M., Abtout, A., Boukerbout, H. & Akacem, N., 2011. Etude de la croûte archéenne du môle In Ouzzal (Hoggar Occidentale) par la méthode gravimétrique: identification des sources par la transformée en ondelettes continues, *Bull. Serv. Geog. Nat.,* **22,** 259–274.

Bouyahiaoui, B. *et al.*, 2015. Crustal structure of the eastern Algerian margin and adjacent deep basin (western Mediterranean) and implications for kinematic reconstructions, *Geophys. J. Int.,* in press.

Brun, J.-P. & Beslier, M.-O., 1996. Mantle exhumation at passive margins, *Earth planet. Sci. Lett.,* **142,** 161–173.

Burov, E.B. & Diament, M., 1995. The effective elastic thickness (Te) of continental lithosphere: what does it really mean? *J. geophys. Res.*, **100**(B3), 3905–3928.

Carlson, R.L. & Herrick, C.N., 1990. Densities and porosities in the oceanic crust and their variations with depth and age, *J. geophys. Res.*, **95,** 9153–9170.

Carminati, E., Wortel, M.J.R., Spakman, W. & Sabadini, R., 1998. The role of slab detachment processes in the opening of the western–central Mediterranean basins: some geological and geophysical evidence, *Earth planet. Sci. Lett.,* **160,** 651–665.

Carminati, E., Lustrino, M. & Dogliono, C., 2012. Geodynamic evolution of the central and western Mediterranean: tectonics vs. igneous petrology constraints, *Tectonophysics,* doi:10.1016/j.tecto.2012.01.026.

Caputo, M., Panza, G.F. & Postpischl, D., 1970. Deep structure of the Mediterranean basin, *J. geophys. Res.,* **75,** 4919–4923.

Cavazza, W., Roure, F., Spakman, W., Stampfli, G.M., Ziegler, P.A. & Grp, T.P.W., 2004. The transmed Atlas: geological-geophysical fabric of the Mediterranean region—final report of the project, *Episodes,* **27,** 244–254.

Cloetingh, S.A.P.L., Wortel, M.J.R. & Vlaar, N.J., 1982. Evolution of passive continental margins and initiation of subduction zones, *Nature,* **297,** 139–142.

Cloetingh, S., Wortel, R. & Vlaar, N.J., 1989. On the initiation of subduction zones, *Pure appl. Geophys.,* **129,** 7–25.

Contrucci, I., Klingelhöfer, F., Perrot, J., Bartolome, R., Gutscher, M.A., Sahabi, M., Malod, J.A. & Réhault, J.P., 2004. The crustal structure of the NW-Moroccan continental margin from wide-angle and reflection seismic data, *Geophys. J. Int.,* **159,** 117–128.

Déverchère, J. *et al.*, 2005. Active thrust faulting offshore Boumerdès, Algeria, and its relations to the 2003 Mw 6.9 earthquake, *Geophys. Res. Lett.,* **32,** doi:10.1029/2004GL021646.

Dewey, J.F., Helman, M.L., Turco, E., Hutron, D.H.W. & Knott, S.D., 1989. Kinematics of Western Mediterranean, in *Alpine Tectonics,* Vol. 45, pp. 265–283, ed. Coward, M.P., Detrich, D. & Park, R.G., Geol. Soc. London, Spec. Publ.

Domzig, A. *et al.*, 2006. Searching for the Africa-Eurasia Miocene boundary onshore Western Algeria (Maradja'03 cruise), *C. R. Geosci.,* **338,** 80–91.

Faccenna, C., Giardini, D., Davy, P. & Argentieri, A., 1999. Initiation of subduction at Atlantic-type margins: insights from laboratory experiments, *J. geophys. Res.,* **104,** 2749–2766.

Faccenna, C., Becker, T.W., Lucente, F.P., Jolivet, L. & Rossetti, F., 2001. History of subduction and back-arc extension in the Central Mediterranean, *Geophys. J. Int.*, **145,** 809–820.

Faccenna, C., Piromallo, C., Crespo-Blanc, A., Jolivet, L. & Rossetti, F., 2004. Lateral slab deformation and the origin of the western Mediterranean arcs, *Tectonics,* **23,** TC1012, doi:10.1029/2002TC001488.

Frizon de Lamotte, D., Andrieux, J. & Guezou, J.C., 1991. Cinématique des chevauchements néogènes dans l'Arc bético-rifain: discussion sur les modèles géodynamiques, *Bull. Soc. Géol. Fr.,* **162,** 611–626.

Frizon de Lamotte, D., Saint Bezar, B.A., Bracene, R. & Mercier, E., 2000. The two main steps of the Atlas building and geodynamics of the western Mediterranean, *Tectonics,* **19,** 740–761.

Frizon de Lamotte, D., Raulin, C., Mouchot, N., Wrobel-Daveau, J.C., Blanpied, C. & Ringenbach, J.C., 2011. The southernmost margin of the Tethys realm during the Mesozoic and Cenozoic: initial geometry and timing of the inversion processes, *Tectonics,* **30,** TC3002, doi:10.1029/2010TC002691.

Gelabert, B., Sabat, F. & Rodriguez-Perea, A., 2002. A new proposal for the late Cenozoic geodynamic evolution of the western Mediterranean, *Terra Nova,* **14,** 93–100.

Gerya, T., 2011. Future directions in subduction modeling, *J. Geodyn.,* **52,** 344–378.

Gueguen, E., Doglioni, C. & Fernandez, M., 1998. On the post-25 Ma geodynamic evolution of the western Mediterranean, *Tectonophysics,* **298,** 259–269.

Gurnis, M., 1992. Rapid continental subsidence following the initiation and evolution of subduction, *Science,* **255,** 1556–1558.

Hamilton, E.L., 1978. Sound velocity-density relations in sea-floor sediments and rocks, *J. acoust. Soc. Am.*, **63,** 366–377.

Idres, M. & Aifa, T., 1995. Some parameters to improve a gravity network accuracy: application to the new reference base stations network of the North of Algeria, *Bull. Serv. Geol. Algerie,* **6,** 79–94.

International Gravimetric Bureau, 2012. IAG Geodesist's Handbook, 2012, *J. Geod.,* **86**(10), Springer, doi:10.1007/s00190-012-0584-1.

Irving, E., 1977. Drift of the major continental blocks since the Devonian, *Nature,* **270,** 304–309.

Irving, E., 2004. The case for Pangea B, and Intra-Pangean Megashear, in *Timescales of the Paleomagnetic Field,* Geophysical Monograph Series 145, pp. 13–27, American Geophysical Union.

Jammes, S. & Huismans, R., 2012. Structural styles of mountain building: controls of lithospheric rheologic stratification and extensional inheritance, *J. geophys. Res.,* **117,** doi:10.1029/2012JB009376.

Jolivet, L., Augier, R., Robin, C., Suc, J.P. & Rouchy, J.M., 2006. Lithospheric-scale geodynamic context of the Messinian salinity crisis, *Sediment. Geol.,* **188–189,** 9–33.

Jolivet, L., Faccenna, C. & Piromallo, C., 2009. From mantle to crust: stretching the Mediterranean, *Earth planet. Sci. Lett.*, **285,** 198–209.

Kherroubi, A., 2011. Etude de la sismicité de l'offshore algérien, *PhD thesis*, Univ. Tlemcen, Algeria, 158 pp.

Kherroubi, A. *et al.*, 2009. Recent and active deformation pattern off the easternmost Algerian margin, Western Mediterranean Sea: new evidence for contractional tectonic reactivation, *Mar. Geol.,* **261**(1), 17–32.

Klingelhoefer, F. *et al.*, 2009. Crustal structure of the SW-Moroccan margin from wide-angle and reflection seismic data (the DAKHLA experiment) Part A: Wide-angle seismic models, *Tectonophysics*, **468,** 63–82.

Klingelhoefer, F. *et al.*, 2010. Limits of the seismogenic zone in the epicentral region of the 26 December 2004 great Sumatra-Andaman earthquake: results from seismic refraction and wide-angle reflection surveys and thermal modeling, *J. geophys. Res.,* **115,** B01304, doi:10.1029/2009JB006569.

Kwon, Y.W. & Bang, H., 2000. *The Finite Element Method Using Matlab,* CRC Press, 624 pp.

Lagabrielle, Y., Labaume, P. & De Saint-Blanquat, M., 2010. Mantle exhumation, crustal denudation and gravity tectonics during Cretaceous rifting in the Pyrenees: new messages from the lherzolite bodies, *Tectonics,* **29,** TC4012, doi:10.1029/2009tC002588.

Le Pichon, X., 1968. Sea-floor spreading and continental drift, *J. geophys. Res.,* **73,** 3661–3697.

Leprêtre, A., Klingelhoefer, F., Graindorge, D., Schnurle, P., Beslier, M.O., Yelles, K., Déverchère, J. & Bracene, R., 2013. Multiphased tectonic evolution of the Central Algerian margin from combined wide-angle and reflection seismic data off Tipaza, Algeria, *J. geophys. Res.,* **118,** 3899–3916.

Lonergan, L. & White, N., 1997. Origin of the Betic-Rif mountain belt, *Tectonics,* **16,** 504–522.

Mauffret, A., 2007. The Northwestrn (Maghreb) Boundary of the Nubia (Africa) Plate, *Tectonophysics,* **429,** 21–44.

Mauffret, A., Frizon de Lamotte, D., Lallemant, S., Gorini, C. & Maillard, A., 2004. E-W opening of the Algerian basin (Western Mediterranean), *Terra Nova*, **16,** 257–264.

Maury, R.C. *et al.*, 2000. Post-collision neogene magmatism of the Mediterranean Maghreb margin: a consequence of slab breakoff, *C.R. Acad. Sci. Paris,* **331,** 159–173.

McKenzie, D., Molnar, P. & Davies, D., 1970. Plate tectonics of the Red Sea and East Africa, *Nature,* **226,** 243–248.

Medaouri, M., Déverchère, J., Graindorge, D., Bracene, R., Badji, R., Ouabadi, A., Yelles-Chaouche, K. & Bendiab, F., 2014. The transition from Alboran to Algerian basins (Western Mediterranean Sea): chronostratigraphy, deep crustal structure and tectonic evolution at the rear of a narrow slab rollback, *J. Geodyn.,* **77,** 186–205.

Mihoubi, A. *et al.*, 2014. Seismic imaging of the eastern Algerian margin off Jijel: integrating wide-angle seismic modeling and multichannel seismic pre-stack depth migration, *Geophys. J. Int.,* **198,** 1486–1503.

Muttoni, G., Kent, D.V. & Channell, J.E.T., 1996. The evolution of Pangea: palaeomagnetic constraints from the Southern Alps, Italy, *Earth planet. Sci. Lett.,* **146,** 107–120.

Niu, Y., O'Hara, M.J.O. & Pearce, J.A., 2003. Initiation of subduction zones as a consequence of lateral compositional buoyancy contrast within the lithosphere: a petrological perspective, *J. Petrol.,* **44,** 851–866.

Olivet, J.L., Bonnin, J., Beuzart, P. & Auzende, J.M., 1982. Cinématique des plaques et paléogéographie: une revue, *Bull. Soc. Géol. Fr.,* **7,** 875–892.

Regenauer-Lieb, K., Yuen, D. & Branlund, J., 2001. The initiation of subduction: criticality by addition of water? *Science,* **294,** 578–580.

Ricou, L.E., 1996. The plate tectonic history of the past Tethys Ocean, in *The Oceans Basins and Margin. The Tethys Ocean,* Vol. **8**, pp. 3–70, eds Nairn, A.E.M., Ricou, L.-E., Vrielynck, B. & Dercourt, J., Plenum Press.

Roca, E., Sans, M., Cabrera, L. & Marzo, M., 1999. Oligocene to Middle Miocene evolution of the central Catalan margin (northwestern Mediterranean), *Tectonophysics,* **315,** 209–233.

Roca, E., 2001. The Northwest-Mediterranean basin (Valencia trough, Gulf of Lions and Liguro-Provencal basins): structure and geodynamic evolution, in *Peri-Tethyan rift/Wrench Basins and Passive Margins,* Vol. **186**, pp. 671–706, eds Ziegler, P.A., Cavazza, W., Robertson, A.F.H. & Crasquin-Soleau, S., Mem. Mus. Nat. Hist. Nat.

Roca, E. *et al.*, 2004. Transmed Transect II, in *The TRANSMED Atlas: The Mediterranean Region from Crust to Mantle,* eds Cavazza, W., Roure, F., Spakman, W., Stampfli, G.M. & Ziegler, P.A., Springer-Verlag.

Rosenbaum, G., Lister, G.S. & Duboz, C., 2002. Reconstruction of the tectonic evolution of the western Mediterranean since the Oligocene, in Reconstruction of the evolution of the Alpine-Himalayan Orogen, edited by G. Rosenbaum, and G.S. Lister, *J. Virtual Explor.,* **8,** 107–126.

Savelli, C., 2002. Time–space distribution of magmatic activity in the western Mediterranean and peripheral orogens during the past 30 Ma (a stimulus to geodynamic considerations), *J. Geodyn.,* **34,** 99–126.

Schettino, A. & Turco, E., 2006. Plate kinematics of the Western Mediterranean region during the Oligocene and Early Miocene, *Geophys. J. Int.,* **166**(3), 1398–1423.

Schettino, A. & Turco, E., 2011. Tectonic history of the western tethys since the late Triassic, *Geol. Soc. Am. Bull.,* **123,** 89–105.

Serpelloni, E., Vannucci, G., Pondrelli, S., Argnani, A., Casula, G., Anzidei, M., Baldi, P. & Gasperini, P., 2007. Kinematics of the Western Africa-Eurasia plate boundary from focal mechanisms and GPS data, *Geophys. J. Int.,* **169,** 1180–1200.

Spakman, W. & Wortel, M.J.R., 2004. A tomographic view on Western Mediterranean Geodynamics, in *The TRANSMED Atlas: The Mediterranean Region from Crust to Mantle,* pp. 31–52, eds Cavazza, W., Roure, F., Spakman, W., Stampfli, G.M. & Ziegler, P., Springer-Verlag.

Stern, R.J., 2004. Subduction initiation: spontaneous and induced, *Earth planet. Sci. Lett.,* **226,** 275–292.

Talwani, M., Fitman, W.C. & Heirtzler, J.R., 1969. Magnetic anomalies in the North Atlantic (abs 406), *Trans. Am. Geophys. Un.,* **50,** 189.

van Hinsbergen, D.J.J., Vissers, R.L.M. & Spakman, W., 2014. Origin and consequences of western Mediterranean subduction, rollback, and slab segmentation, *Tectonics,* **33,** 393–419.

Verges, J. & Sabat, F., 1999. Constraints on the Western Mediterranean kinematics evolution along a 1000-km transect from Iberia to Africa, in *The Mediterranean Basin: Tertiary Extensions within the Alpine Orogen,* Vol. 156, pp. 63–80, eds Durand, B., Jolivet, L., Horvath, F. & Séranne, M., Geol. Soc. Spec. Publ.

Watts, A.B., 1981. The U.S. Atlantic continental margin: subsidence history, crustal structure and thermal evolution, American Assoc. Petrol. Geol. Education Course #19, 75 pp.

Watts, A.B., 1992. The effective elastic thickness of the lithosphere and the evolution of foreland basins, *Basin Res.,* **4,** 169–178.

Watts, A.B., 2001. *Isostasy and Flexure of the Lithosphere,* 458 pp., Cambridge Univ. Press.

Watts, A.B. & Burov, E.B., 2003. Lithospheric strength and its relationship to the elastic and seismogenic thickness, *Earth planet. Sci. Lett.,* **213,** 113–131.

Yelles, A. *et al.*, 2009. Plio-Quaternary reactivation of the Neogene margin off NW Algiers, Algeria: the Khayr al Din bank, *Tectonophysics,* **475,** 98–116.

Yelles-Chaouche, A.K., Boudiaf, A., Djellit, H. & Bracène, R., 2006. La tectonique active de la région nord-algérienne, *C.R. Geosci.,* **338,** 126–139.

Zhu, G., Gerya, T.V., Yuen, D.A., Honda, S., Yoshida, T. & Connolly, J.A.D., 2009. 3-D dynamics of hydrous thermalchemical plumes in oceanic subduction zones, *Geochem. Geophys. Geosyst.,* **10,** Q11006, doi:10.1029/2009GC002625.

SUPPORTING INFORMATION

Additional Supporting Information may be found in the online version of this paper:

Figure 1. Topography, bathymetry by ETOPO1 1-min global relief (www.ngdc.noaa.gov) and seismicity of the Algerian margin (epicentres and focal mechanisms). Solid lines indicate the location of the SPIRAL wide-angle profiles. Inset shows a more regional

tectonic sketch of the Mediterranean Region (modified after Barrier *et al.* 2004).

Figure 2. Free air anomaly map of northern Algeria. Solid lines mark the SPIRAL wide-angle seismic profiles (TI = Tipaza, KA = Greater Kabylia, JI = Jijel, AN = Annaba).

Figure 3. Setup of the flexural models. *Te* is the effective elastic thickness in km. The deflection (*w*) is set to zero at the extremities of the plates, and imposed at the plate junction.

Figure 4. (a) Topography and bathymetry for the Tipaza profile. (b) Free-air anomaly. Dotted red line corresponds to measured gravity. Solid green and blue lines are predicted free-air anomalies using different parameters for the sediments, the upper crust, and the lower crust and mantle (Conversion 1) or using only Birch's law (conversion 2), respectively. (c) Density model calculated by converting the seismic velocities into densities with Birch's law (seismic velocities after Leprêtre *et al.* 2013). (d) 2-D flexural model of the Tipaza profile. Green and blue lines are the computed deflection corresponding to the two different velocity–density conversions, and black line is the modelled deflection. Thick vertical lines delimitate the transition zone between the two flexed plates. (http://gji.oxfordjournals.org/lookup/suppl/doi:10.1093/gji/ggv098/-/DC1)